European Journal of Mechanics B/Fluids 28 (2009) 185–190

Contents lists available at ScienceDirect

European Journal of Mechanics B/Fluids

www.elsevier.com/locate/ejmflu

Heat transfer in the flow of a cold, two-dimensional draining sheet over a hot, horizontal cylinder

Jian-Jun Shu *, Graham Wilks

School of Mechanical & Aerospace Engineering, Nanyang Technological University, 50 Nanyang Avenue, Singapore 639798

ARTICLE INFO

Article history:
Received 9 January 2007
Received in revised form 26 November 2007
Accepted 7 April 2008
Available online 11 April 2008

Keywords:
Heat transfer
Thin film flow
Large Reynolds numbers and modified
Keller box method

ABSTRACT

The paper considers heat transfer characteristics of thin film flow over a hot horizontal cylinder resulting from a cold vertical sheet of liquid falling onto the surface. The underlying physical features of the developing film thickness, velocity and temperature distributions have been illustrated by numerical solutions of high accuracy for large Reynolds numbers using the modified Keller box method. The solutions for film thickness distribution are good agreement with those obtained using the Pohlhausen integral momentum technique thus providing a basic confirmation of the validity of the results presented.

1. Introduction

The draining flow under gravity falling across a horizontal cylinder occurs frequently in a variety of industrial heat-transfer applications, such as heat exchange in water desalinization apparatus [1], in absorption coolers [2], in power and process condensers [3] and in thin film cooling [4]. In order to understand the operations and, in particular, the efficiency of these processes, it is important to have a detailed study of such a flow and has been the subject of numerous theoretical and experimental research studies reported in the literature. Comprehensive literature reviews of such draining flow studies have been made by Thome [5] and Ribatski and Jacobi [6] to reveal fully the developments in this subject.

Mitrovic [7] pointed out that the transition of draining flow patterns, such as droplet, column or sheet, was dependent on flow rates. At a high flow rate, the draining flow pattern may be in the form of sheet. It is natural to a closer inspection of the draining sheet flow pattern. However previous studies of such draining sheet flow over a horizontal cylinder have been concerned with the purely hydrodynamic problem. Abdelghaffer et al. [8] obtained an approximation using the Pohlhausen integral momentum technique, which assumed an approximate velocity profile across the thickness of the film; Hunt [9] obtained a numerical solution using the modified Keller box method, which accommodated the outer, free boundary. Heat-transfer characteristics of the flow have not been considered.

In this paper, the heat transfer in the flow of a cold, two-dimensional draining sheet over a hot, horizontal cylinder is investigated. The accurate and comprehensive numerical solutions for both velocity and temperature distributions is obtained.

2. Modelling

The problem to be examined concerns the film cooling which occurs when a cold vertically draining sheet strikes a hot horizontal cylinder. Although a sheet of fluid draining under gravity is accelerated and thin at impact [10,11], it is reasonable to model the associated volume flow as a sheet of uniform velocity U_0, uniform temperature T_0 and semi-thickness H_0 as is illustrated in Fig. 1. The notation $Q = U_0 H_0$ is introduced for the flow rate and a film Reynolds number may be defined as $R_e = U_0 a/\nu$ based on the cylinder radius where ν is the kinematic viscosity of the fluid and a is the radius of the cylinder.

3. Governing equations

The flow under investigation has been modelled as a steady, two-dimensional flow of incompressible fluid. In the absence of viscous dissipation, the equations expressing conservation of mass, momentum and energy are consequently

$$\frac{\partial v_\theta}{\partial \theta} + \frac{\partial}{\partial r}(r v_r) = 0, \tag{1}$$

$$\frac{v_\theta}{r}\frac{\partial v_\theta}{\partial \theta} + v_r \frac{\partial v_\theta}{\partial r} + \frac{v_r v_\theta}{r} = g\sin\theta - \frac{1}{\rho r}\frac{dP}{d\theta} + \frac{\mu}{\rho}\left[\frac{1}{r}\frac{\partial}{\partial r}\left(r\frac{\partial v_\theta}{\partial r}\right) + \frac{1}{r^2}\frac{\partial^2 v_\theta}{\partial \theta^2} + \frac{2}{r^2}\frac{\partial v_r}{\partial \theta} - \frac{v_\theta}{r^2}\right], \tag{2}$$

* Corresponding author.
E-mail address: mjjshu@ntu.edu.sg (J.-J. Shu).

0997-7546/$ – see front matter
doi:10.1016/j.euromechflu.2008.04.001

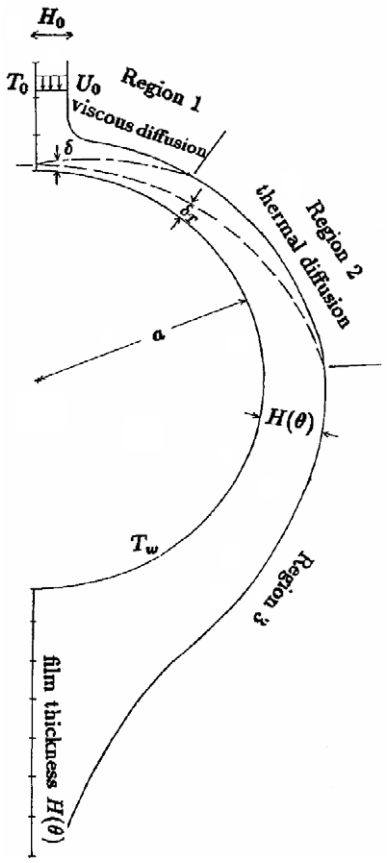

Fig. 1. The vertical sheet and resultant film for the cylinder.

$$\frac{\nu_\theta}{r}\frac{\partial T}{\partial \theta}+\nu_r\frac{\partial T}{\partial r}=\frac{k}{\rho C_p}\left[\frac{1}{r}\frac{\partial}{\partial r}\left(r\frac{\partial T}{\partial r}\right)+\frac{1}{r^2}\frac{\partial^2 T}{\partial \theta^2}\right] \tag{3}$$

where $\vec{V}=(\nu_\theta,\nu_r)$ are velocity components associated with cylindrical coordinates (θ,r) measured the angular displacement from the top of the cylinder and the radial distance from the centre of the cylinder respectively. ρ, μ, C_p and k are the density, dynamic viscosity, specific heat at constant pressure and the thermal conductivity of the cooling fluid in the sheet respectively. T and P are respectively the temperature and pressure within the fluid.

In the specified physical setting, the equations are to be solved subject to the following conditions.

(i) The no slip boundary condition at the cylinder wall requires that

$$\nu_\theta=\nu_r=0 \quad \text{on } r=a,\ 0\leqslant\theta\leqslant\pi. \tag{4}$$

(ii) The temperature at the cylinder wall is assumed constant as T_w, say i.e.

$$T=T_w \quad \text{on } r=a,\ 0\leqslant\theta\leqslant\pi. \tag{5}$$

(iii) On the free surface of the film, prescribed by $r=a+H(\theta)$, the shearing stress may be assumed negligible and consequently

$$r\frac{\partial}{\partial r}\left(\frac{\nu_\theta}{r}\right)+\frac{1}{r}\frac{\partial \nu_r}{\partial \theta}=0 \quad \text{at } r=a+H(\theta),\ 0\leqslant\theta\leqslant\pi. \tag{6}$$

(iv) Similarly, in a film cooling environment such as water surrounded by air, it may be assumed that there is negligible heat flux on the free surface and hence that

$$\frac{\partial T}{\partial r}=0 \quad \text{at } r=a+H(\theta),\ 0\leqslant\theta\leqslant\pi. \tag{7}$$

(v) Once an overall flow rate $Q=U_0H_0$ has been prescribed, a conservation of volume flow constraint at any given θ station leads to the condition

$$\int_a^{a+H(\theta)}\nu_\theta(\theta,r)\,dr=\text{constant}=H_0U_0 \quad \text{for } 0\leqslant\theta\leqslant\pi. \tag{8}$$

Under the assumption that the film thickness remains thin relative to a characteristic horizontal dimension, a boundary layer treatment of the equations leads to significant simplification.

The following non-dimensional variables are introduced

$$x=\theta,\quad y=\frac{R_e^{1/2}(r-a)}{a},\quad \bar{h}(x)=\frac{R_e^{1/2}H(\theta)}{a},$$
$$\bar{U}=\frac{\nu_\theta}{U_0},\quad \bar{V}=\frac{R_e^{1/2}\nu_r}{U_0},\quad \bar{\phi}=\frac{T-T_w}{T_0-T_w},\quad p=\frac{P}{\rho U_0^2}. \tag{9}$$

In the limit $R_e\to+\infty$ with x remaining O(1) and after neglecting terms of $O(\frac{1}{R_e^{1/2}})$ compared with unity, the following equations are obtained

$$\frac{\partial \bar{U}}{\partial x}+\frac{\partial \bar{V}}{\partial y}=0, \tag{10}$$

$$\bar{U}\frac{\partial \bar{U}}{\partial x}+\bar{V}\frac{\partial \bar{U}}{\partial y}=\frac{1}{F_r}\sin x-\frac{dp}{dx}+\frac{\partial^2\bar{U}}{\partial y^2}, \tag{11}$$

$$P_r\left(\bar{U}\frac{\partial \bar{\phi}}{\partial x}+\bar{V}\frac{\partial \bar{\phi}}{\partial y}\right)=\frac{\partial^2\bar{\phi}}{\partial y^2} \tag{12}$$

where $P_r=\nu/\kappa$ is the Prandtl number with ν the kinematic viscosity μ/ρ and κ the thermometric conductivity $k/(\rho C_p)$, and $F_r=U_0^2/(ag)$ is the Froude number based on the sheet velocity on its surface. In common with standard boundary layer theory equation implies that the pressure across the film remains constant. In the absence of external pressure gradients and with zero shear assumed on the free surface, the pressure term in (11) is identically zero.

The boundary conditions now read

(i) $$\bar{U}=\bar{V}=0 \quad \text{on } y=0,\ 0\leqslant x\leqslant\pi, \tag{13}$$

(ii) $$\bar{\phi}=0 \quad \text{on } y=0,\ 0\leqslant x\leqslant\pi, \tag{14}$$

(iii) $$\frac{\partial \bar{U}}{\partial y}=0 \quad \text{at } y=\bar{h}(x),\ 0\leqslant x\leqslant\pi, \tag{15}$$

(iv) $$\frac{\partial \bar{\phi}}{\partial y}=0 \quad \text{at } y=\bar{h}(x),\ 0\leqslant x\leqslant\pi, \tag{16}$$

(v) $$\int_0^{\bar{h}(x)}\bar{U}\,dy=\frac{R_e^{1/2}H_0}{a} \quad \text{for } 0\leqslant x\leqslant\pi. \tag{17}$$

Approximations of equations equivalent to (10)–(11) under boundary conditions (13), (15) and (17) have been outlined by Abdelghaffer et al. [8].

4. Numerical solutions

The continuity equation (10) can be eliminated by introducing a stream function ψ defined by

$$\bar{U}=\frac{\partial \psi}{\partial y},\qquad \bar{V}=-\frac{\partial \psi}{\partial x}. \tag{18}$$

Substituting Eq. (18) into (10)–(17) gives

$$\frac{\partial^3\psi}{\partial y^3}+\frac{1}{F_r}\sin x=\frac{\partial \psi}{\partial y}\frac{\partial^2\psi}{\partial x\partial y}-\frac{\partial \psi}{\partial x}\frac{\partial^2\psi}{\partial y^2}, \tag{19}$$

$$\frac{\partial^2\bar{\phi}}{\partial y^2}=P_r\left(\frac{\partial \psi}{\partial y}\frac{\partial \bar{\phi}}{\partial x}-\frac{\partial \psi}{\partial x}\frac{\partial \bar{\phi}}{\partial y}\right) \tag{20}$$

subject to boundary conditions

$$\psi = 0, \quad \frac{\partial \psi}{\partial y} = 0, \quad \bar{\phi} = 0 \quad \text{on } y = 0,\ 0 \leqslant x \leqslant \pi, \tag{21}$$

$$\psi = \frac{R_e^{1/2} H_0}{a}, \quad \frac{\partial^2 \psi}{\partial y^2} = 0, \quad \frac{\partial \bar{\phi}}{\partial y} = 0 \quad \text{at } y = \bar{h}(x),\ 0 \leqslant x \leqslant \pi, \tag{22}$$

$$\bar{h} = \frac{R_e^{1/2} H_0}{a}, \quad \psi = y, \quad \bar{\phi} = 1 \quad \text{on } x = 0,\ 0 < y \leqslant \frac{R_e^{1/2} H_0}{a} \tag{23}$$

where the initial condition (23) appears due to the original initial condition

$$H = H_0, \quad \nu_0 = U_0, \quad T = T_0 \quad \text{on } \theta = 0,\ a < r \leqslant a + H_0. \tag{24}$$

In anticipation of the use of a Keller box method and its attractive extrapolation features the differential system (19)–(23) is re-cast as the following first order system

$$\begin{aligned}
&\frac{\partial \psi}{\partial y} = \bar{u},\\
&\frac{\partial \bar{u}}{\partial y} = \bar{v},\\
&\frac{\partial \bar{v}}{\partial y} = -\frac{1}{F_r} \sin x + \bar{u} \frac{\partial \bar{u}}{\partial x} - \bar{v} \frac{\partial \psi}{\partial x},\\
&\frac{\partial \bar{\phi}}{\partial y} = \bar{w},\\
&\frac{\partial \bar{w}}{\partial y} = P_r \left(\bar{u} \frac{\partial \bar{\phi}}{\partial x} - \bar{w} \frac{\partial \psi}{\partial x} \right)
\end{aligned} \tag{25}$$

whose boundary conditions are

$$\begin{aligned}
&\psi = 0, \quad \bar{u} = 0, \quad \bar{\phi} = 0 \quad \text{on } y = 0,\ 0 \leqslant x \leqslant \pi,\\
&\psi = \frac{R_e^{1/2} H_0}{a}, \quad \bar{v} = 0, \quad \bar{w} = 0 \quad \text{on } y = \bar{h}(x),\ 0 \leqslant x \leqslant \pi,\\
&\bar{h} = \frac{R_e^{1/2} H_0}{a}, \quad \psi = y, \quad \bar{\phi} = 1 \quad \text{on } x = 0,\ 0 < y \leqslant \frac{R_e^{1/2} H_0}{a}.
\end{aligned} \tag{26}$$

If these equations were used as the basis of solution there would be strong comparisons between the associated algorithm and that developed in [12]. However the expectation of an initial Blasius boundary layer within the film can be assimilated into the solution scheme by further transformations. The underlying methodology of solution nevertheless remains the same. In each case the discretization is aimed at generating a simultaneous system of non-linear equations which can be solved by Newton iteration.

According to the non-dimensional transformation, the boundary layer thickness grows like $x^{1/2}$ for small x in the y direction.

The following coordinate transformation, what simultaneously maps the film thickness onto the unit interval and removes the Blasius singularity at the origin, is introduced

$$x = \xi^2, \qquad y = \frac{\xi \eta \bar{h}}{\xi + 1 - \eta}.$$

The dependent variables are transformed as

$$\begin{aligned}
&\psi = \frac{\xi}{\xi + 1 - \eta} f, \quad \bar{u} = u, \quad \bar{v} = \frac{\xi + 1 - \eta}{\xi} v,\\
&\bar{\phi} = \phi, \quad \bar{w} = \frac{\xi + 1 - \eta}{\xi} w, \quad \bar{h} = h.
\end{aligned}$$

The equations to be solved now read

$$\begin{aligned}
f_\eta &= \frac{(1+\xi) h u}{\xi + 1 - \eta} - \frac{f}{\xi + 1 - \eta},\\
u_\eta &= \frac{(1+\xi) h v}{\xi + 1 - \eta},\\
v_\eta &= \frac{v}{\xi + 1 - \eta} - \frac{\xi^2 (1+\xi) h \sin(\xi^2)}{(\xi + 1 - \eta)^3 F_r} - \frac{(1-\eta)(1+\xi) h f v}{2(\xi + 1 - \eta)^4}\\
&\quad + \frac{\xi (1+\xi) h}{2(\xi + 1 - \eta)^3} (u u_\xi - v f_\xi),\\
\phi_\eta &= \frac{(1+\xi) h w}{\xi + 1 - \eta},\\
w_\eta &= \frac{w}{\xi + 1 - \eta} - \frac{P_r (1-\eta)(1+\xi) h f w}{2(\xi + 1 - \eta)^4}\\
&\quad + \frac{P_r \xi (1+\xi) h}{2(\xi + 1 - \eta)^3} (u \phi_\xi - w f_\xi)
\end{aligned} \tag{27}$$

subject to

$$\begin{aligned}
&f = 0, \quad u = 0, \quad \phi = 0 \quad \text{on } \eta = 0,\ 0 \leqslant \xi \leqslant \sqrt{\pi},\\
&f = \frac{R_e^{1/2} H_0}{a}, \quad v = 0, \quad w = 0 \quad \text{on } \eta = 1,\ 0 \leqslant \xi \leqslant \sqrt{\pi},\\
&h = \frac{R_e^{1/2} H_0}{a}, \quad f = f_0(\eta), \quad \phi = \phi_0(\eta) \quad \text{on } \xi = 0,\ 0 < \eta \leqslant 1
\end{aligned} \tag{28}$$

where the initial profiles $f_0(\eta)$ and $\phi_0(\eta)$ are found by putting $\xi = 0$ and $h = \frac{R_e^{1/2} H_0}{a}$ into (27) and solving, subject to conditions $f = u = \phi = 0$ at $\eta = 0$ and $u = 1$, $\phi = 1$ at $\eta = 1$.

The parabolic system of equations and boundary conditions (27)–(28) has been solved by marching in the ξ-direction using a modification of the Keller box method. A non-uniform grid is placed on the domain $\xi \geqslant 0$, $0 \leqslant \eta \leqslant 1$ and the resulting difference equations are solved by Newton iteration. Solutions are obtained on different sized grids and Richardson's extrapolation used to produce results of high accuracy.

It is worth to mention to this end that the general equations describing parabolic free boundary problems arising from thin film flows [12] are

$$\frac{\partial^3 \psi}{\partial y^3} + F(x) = G^2(x) \left(\frac{\partial \psi}{\partial y} \frac{\partial^2 \psi}{\partial x \partial y} - \frac{\partial \psi}{\partial x} \frac{\partial^2 \psi}{\partial y^2} \right), \tag{29}$$

$$\frac{\partial^2 \bar{\phi}}{\partial y^2} = P_r G^2(x) \left(\frac{\partial \psi}{\partial y} \frac{\partial \bar{\phi}}{\partial x} - \frac{\partial \psi}{\partial x} \frac{\partial \bar{\phi}}{\partial y} \right) \tag{30}$$

subject to boundary conditions

$$\psi = 0, \quad \frac{\partial \psi}{\partial y} = 0, \quad \bar{\phi} = 0 \quad \text{on } y = 0,\ 0 \leqslant x \leqslant x_s, \tag{31}$$

$$\psi = \gamma, \quad \frac{\partial^2 \psi}{\partial y^2} = 0, \quad \frac{\partial \bar{\phi}}{\partial y} = 0 \quad \text{at } y = \bar{h}(x),\ 0 \leqslant x \leqslant x_s, \tag{32}$$

$$\bar{h} = \gamma, \quad \psi = y, \quad \bar{\phi} = 1 \quad \text{on } x = 0,\ 0 < y \leqslant \gamma. \tag{33}$$

Accordingly the variables are transformed from (x, y) to (ξ, η) by using

$$x = \xi^\alpha, \qquad y = \frac{\xi \eta \bar{h}}{\xi + 1 - \eta}.$$

The dependent variables are transformed as

$$\begin{aligned}
&\psi = \frac{\xi}{\xi + 1 - \eta} f, \quad \bar{u} = \frac{1}{(1+\xi)^\beta} u, \quad \bar{v} = \frac{\xi + 1 - \eta}{\xi (1+\xi)^{2\beta}} v, \quad \bar{\phi} = \phi,\\
&\bar{w} = \frac{\xi + 1 - \eta}{\xi (1+\xi)^\beta} w, \quad \bar{h} = (1+\xi)^\beta h.
\end{aligned}$$

Table 1
Film thickness, free surface velocity and temperature for the cylinder with $F_r = 1$, $\gamma = 1$ and $P_r = 2$

x	film thickness $\bar{h}(x)$	free surface velocity $\bar{u}(x, \bar{h}(x))$	free surface temperature $\bar{\phi}(x, \bar{h}(x))$
0.000	1.000	1.000	1.000
1.115×10^{-2}	1.182	1.000	1.000
3.361×10^{-2}	1.314	1.000	1.000
6.265×10^{-2}	1.426	0.998	1.000
0.105	1.541	0.981	0.999
0.211	1.717	0.914	0.983
0.301	1.796	0.868	0.957
0.501	1.836	0.823	0.885
0.714	1.767	0.840	0.801
1.054	1.611	0.917	0.665
1.303	1.527	0.972	0.573
1.588	1.474	1.013	0.478
2.029	1.472	1.021	0.359
2.545	1.608	0.946	0.261
2.985	1.953	0.800	0.206
π	2.218	0.722	0.191

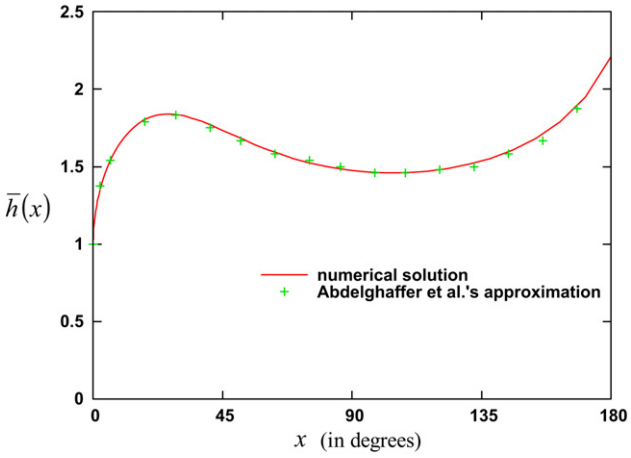

Fig. 2. Film thickness for the numerical solution and Abdelghaffer et al.'s approximation at $F_r = 1$ and $\gamma = 1$.

A full account of the numerical method and the details of implementation are beyond the scope of this paper and will be reported separately [12]. For the cylinder in this paper, the relevant physical parameters should be chosen as

$$F(x) = \frac{1}{F_r}\sin x, \quad G(x) = 1, \quad x_s = \pi, \quad \gamma = \frac{R_e^{1/2} H_0}{a},$$
$$\alpha = 2, \quad \beta = 0.$$

The solution scheme was successfully tested against previously reported results [13–20].

5. Results

A typical run has a coarse grid of dimensions 60×48 in the (ξ, η) domain with each cell being divided into $1, 2, 3$ and 4 subcells respectively. Because of the coordinate singularity at $\xi = 0$, $\eta = 1$, a non-uniform grid is employed and given by $\xi = \bar{\xi}^{1.5}$, $\eta = 1 - (1 - \bar{\eta})^{1.5}$ where $\bar{\xi}$ and $\bar{\eta}$ are uniform. When $\Delta\bar{\xi} \equiv \frac{1}{59}\pi^{\frac{1}{3}}$ and $\Delta\bar{\eta} \equiv \frac{1}{47}$, this gives $\Delta\xi \sim 0.004$ and $\Delta\eta \sim 0.003$ near the singularity, which is sufficiently small to give good accuracy. From the convergence of the extrapolation process previously described the absolute error is 2×10^{-7}. A typical set of numerical data is presented in Table 1.

In Fig. 2, the film thickness distribution around the cylinder is plotted from the numerical solution for $F_r = 1$ and $\gamma = 1$ and individual points calculated by Abdelghaffer et al. [8] using the approximate theory are included on the graph. The agreement is seen to be remarkably good. Figs. 3–9 depict the flavour of the numerical results. Figs. 3–4, 5–6 and 7–9 show film thickness, free surface velocity and free surface temperature respectively for various cases.

For the cylindrical case, the velocity of the flow is controlled by two opposing forces, viscosity trying to slow it down and gravity trying to speed it up. The gravitational component of force affect-

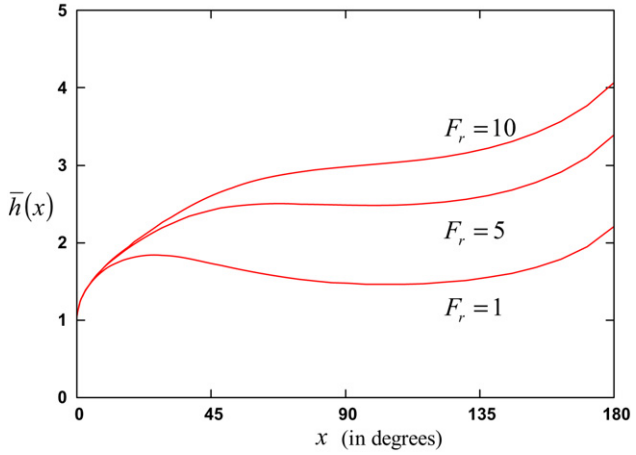

Fig. 3. Film thickness for various Froude numbers at $\gamma = 1$.

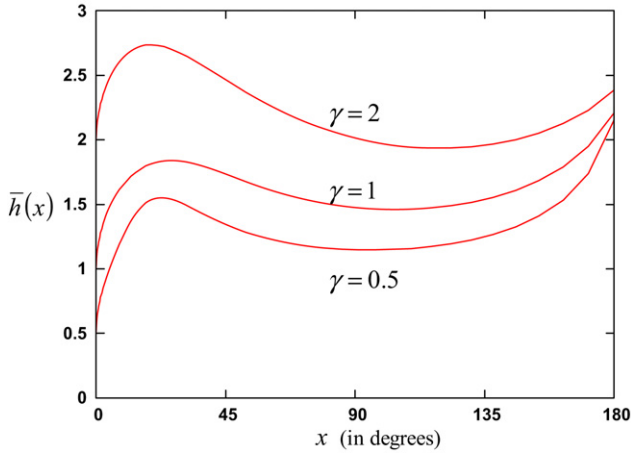

Fig. 4. Film thickness for various values of the parameter γ at $F_r = 1$.

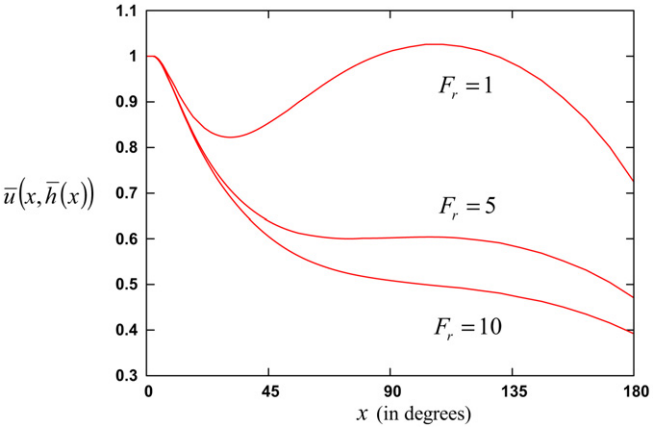

Fig. 5. Free surface velocity for various Froude numbers at $\gamma = 1$.

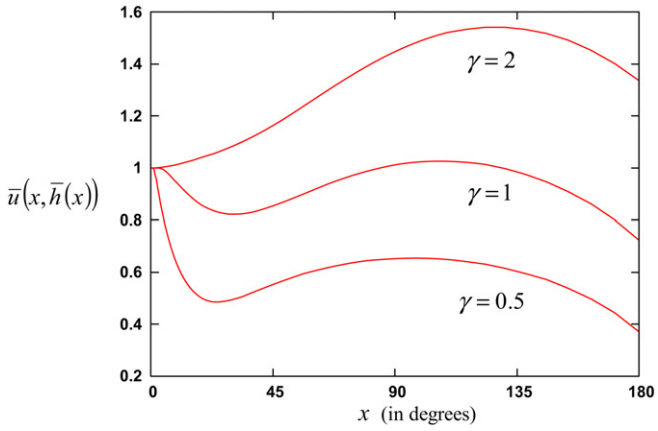

Fig. 6. Free surface velocity for various values of the parameter γ at $F_r = 1$.

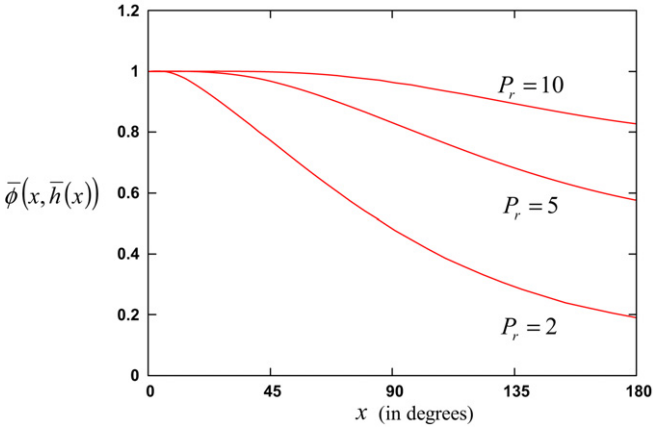

Fig. 7. Free surface temperature for various Prandtl numbers at $F_r = 1$ and $\gamma = 1$.

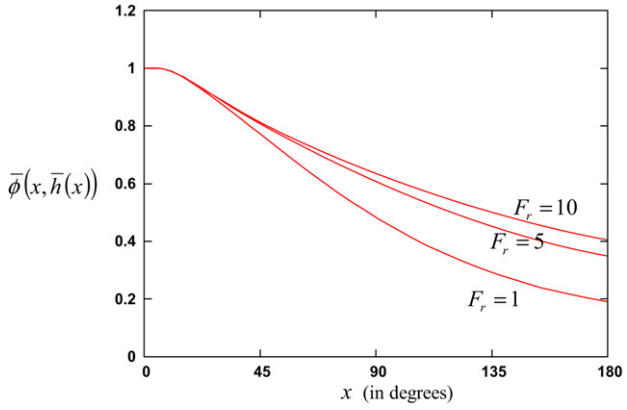

Fig. 8. Free surface temperature for various Froude numbers at $\gamma = 1$ and $P_r = 2$.

ing the flow is greatest near $x = \frac{\pi}{2}$ and least near $x = 0$ and $x = \pi$. Figs. 5–6 show that free surface velocity initially has a slight decrease, followed by a sharp increase as gravity starts to dominate, and finally a gradual decrease is observed as the bottom of the cylinder is approached. This corresponds to the up-down-up situation for the film thickness in Figs. 2–4, and the decline at the different rates for the free surface temperature in Figs. 7–9. As F_r decreases, the effect of gravity increases and hence the thin film thickness, high velocity and low temperature appear corresponding to the small F_r values. As γ decreases, the amount of fluid in the impinging sheet decreases and the ensuing film becomes thinner.

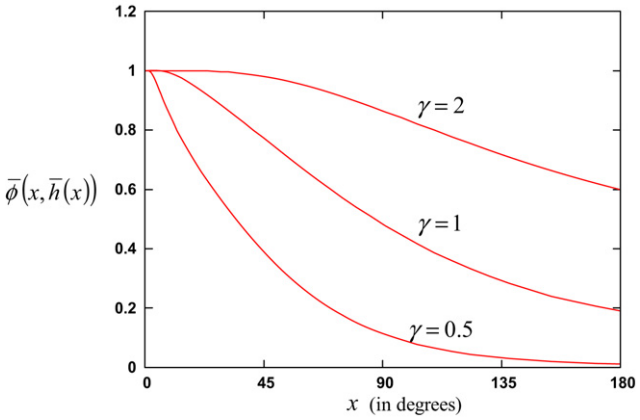

Fig. 9. Free surface temperature for various values of the parameter γ at $F_r = 1$ and $P_r = 2$.

The effect of initial viscosity increases and hence the initial velocity and temperature decreases become sharper as γ decreases. When γ is greater than a certain value, e.g., $\gamma = 2$ for $F_r = 1$, Fig. 6 shows no decrease for the initial velocity. As P_r increases, the temperature decrease becomes more gradual.

6. Concluding remarks

A detailed examination of a draining sheet flow over a horizontal cylinder has been performed. Comprehensive numerical solutions for establishing the flow and heat transfer characteristics of a cold, two-dimensional draining sheet over a hot, horizontal cylinder have been presented. The gross features of such flows have been illustrated over a range of representative parameter values. These indicate the underlying features of the developing film thickness, velocity and temperature distributions. In a practical setting, appropriate parameter values may be evaluated and the design characteristics readily identified from the numerical solutions. In practice, it is not obvious that uniform wetting of the cylinder would occur. Instabilities may distort or even disrupt such a uniform distribution. Nevertheless for a given overall flow rate, the model may represent a valuable first approximation to the aggregate properties of the flow.

References

[1] L.S. Fletcher, V. Sernas, W.H. Parken, Evaporation heat transfer coefficients for thin sea water films on horizontal tubes, Industrial & Engineering Chemistry Process Design and Development 14 (4) (1975) 411–416.
[2] J.W. Andber, G.C. Vliet, Absorption of vapors into liquid films flowing over cooled horizontal tubes, in: Heat Transfer 1986, Proceedings of the eighth International Heat Transfer Conference San Francisco, CA, USA, 1986.
[3] P.J. Marto, R.H. Nunn, Power Condenser Heat Transfer Technology: Computer Modeling/Design/Fouling, Hemisphere Publishing Corporation, 1981.
[4] J.T. Rogers, Laminar falling film flow and heat transfer characteristics on horizontal tubes, The Canadian Journal of Chemical Engineering 59 (2) (1981) 213–222.
[5] J.R. Thome, Falling film evaporation: State-of-the-art review of recent work, Journal of Enhanced Heat Transfer 6 (2–4) (1999) 263–277.
[6] G. Ribatski, A.M. Jacobi, Falling-film evaporation on horizontal tubes – A critical review, International Journal of Refrigeration – Revue Internationale du Froid 28 (5) (2005) 635–653.
[7] J. Mitrovic, Influence of tube spacing and flow rate on heat transfer from a horizontal tube to a falling liquid film, in: Proceedings of the Eighth International Heat Transfer Conference, San Francisco, 4, 1986, 1949–1956.
[8] M.A. Abdelghaffer, A.A. Nicol, R.J. Gribben, G. Wilks, Thin film inundation flow over a horizontal cylinder, Mathematical Engineering Industry 2 (2) (1989) 143–155.
[9] R. Hunt, The numerical solution of parabolic free boundary problems arising from thin film flows, Journal of Computational Physics 84 (2) (1989) 377–402.

[10] J.-J. Shu, Impact of an oblique breaking wave on a wall, Physics of Fluids 16 (3) (2004) 610–614.
[11] J.-J. Shu, Slamming of a breaking wave on a wall, Physical Review E 70 (6) (2004) 066306.
[12] J.-J. Shu, G. Wilks, An accurate numerical method for systems of differentio-integral equations associated with multiphase flow, Computers & Fluids 24 (6) (1995) 625–652.
[13] J.-J. Shu, G. Wilks, Mixed-convection laminar film condensation on a semi-infinite vertical plate, Journal of Fluid Mechanics 300 (1995) 207–229.
[14] J.-J. Shu, G. Wilks, Heat transfer in the flow of a cold, two-dimensional vertical liquid jet against a hot, horizontal plate, International Journal of Heat and Mass Transfer 39 (16) (1996) 3367–3379.
[15] J.-J. Shu, I. Pop, Inclined wall plumes in porous media, Fluid Dynamics Research 21 (4) (1997) 303–317.
[16] J.-J. Shu, I. Pop, Transient conjugate free convection from a vertical flat plate in a porous medium subjected to a sudden change in surface heat flux, International Journal of Engineering Science 36 (2) (1998) 207–214.
[17] J.-J. Shu, I. Pop, On thermal boundary layers on a flat plate subjected to a variable heat flux, International Journal of Heat and Fluid Flow 19 (1) (1998) 79–84.
[18] J.-J. Shu, I. Pop, Thermal interaction between free convection and forced convection along a vertical conducting wall, Heat and Mass Transfer 35 (1) (1999) 33–38.
[19] J.-J. Shu, Microscale heat transfer in a free jet against a plane surface, Superlattices and Microstructures 35 (3–6) (2004) 645–656.
[20] J.-J. Shu, G. Wilks, Heat transfer in the flow of a cold, axisymmetric vertical liquid jet against a hot, horizontal plate, Journal of Heat Transfer – Transactions of the ASME 130 (1) (2008) 012202.